NASA TN D-458

TECHNICAL NOTE
D-458

EXPERIMENTAL SMOKE AND ELECTROMAGNETIC ANALOG STUDY OF INDUCED FLOW FIELD ABOUT A MODEL ROTOR IN STEADY FLIGHT WITHIN GROUND EFFECT

By Robin B. Gray

Georgia Institute of Technology

NATIONAL AERONAUTICS AND SPACE ADMINISTRATION

WASHINGTON

August 1960

1T

NATIONAL AERONAUTICS AND SPACE ADMINISTRATION

TECHNICAL NOTE D-458

EXPERIMENTAL SMOKE AND ELECTROMAGNETIC ANALOG STUDY OF INDUCED FLOW FIELD ABOUT A MODEL ROTOR IN STEADY FLIGHT WITHIN GROUND EFFECT

By Robin B. Gray

SUMMARY

Hovering and steady low-speed forward-flight tests were run on a 4-foot-diameter rotor at a ground height of 1 rotor radius. The two blades had a 2 to 1 taper ratio and were mounted in a see-saw hub. The solidity ratio was 0.05. Measurements were made of the rotor rpm, collective pitch, and forward-flight velocity. Smoke was introduced into the tip vortex and the resulting vortex pattern was photographed from two positions. Using the data obtained from these photographs, wire models of the tip vortex configurations were constructed and the distribution of the normal component of induced velocity at the blade feathering axis that is associated with these tip vortex configurations was experimentally determined at 45° increments in azimuth position from this electromagnetic analog.

Three steady-state conditions were analyzed. The first was hovering flight; the second, a flight velocity just under the wake "tuck under" speed; and the third, a flight velocity just above this speed. These corresponded to advance ratios of 0, 0.022, and 0.030 (or ratios of forward velocity to calculated hovering induced velocity of approximately 0, 0.48, and 0.65), respectively, for the model test rotor.

Cross sections of the wake at 45° intervals in azimuth angle as determined from the path of the tip vortex are presented graphically for all three cases. The nondimensional normal component of the induced velocity that is associated with the tip vortex as determined by an electromagnetic analog at 45° increments in azimuth position and at the blade feathering axis is presented graphically. It is shown that the mean value of this component of the induced velocity is appreciably less after tuck-under than before. It is concluded that this method yields results of engineering accuracy and is a very useful means of studying vortex fields.

INTRODUCTION

The effect of the proximity of the ground causes various changes in the flight characteristics of helicopter rotors which are usually attributed to the changes in the flow pattern underneath the rotor. For instance, it has been shown both theoretically and experimentally that the power required to operate within ground effect is less than that required out of ground effect due to the decrease in the mean normal component of induced velocity at the rotor disk. Other phenomena observed have been the rather sudden increase in lift at certain low forward speeds in the transition regime from hovering to forward flight within ground effect and vice versa in the landing maneuver. By pilot observation, these effects have been qualitatively correlated with the "tucking under" of the rotor wake in takeoff and the reestablishment of the "spreading wake" in landing. Various helicopters have experienced stability and control difficulties when operating at low speeds within ground effect. Reference 1 reports the measurement of very high vibratory blade bending and torsional moments in the transition and low-speed approaches within ground effect and presumes that the cause is the rapid change in flow characteristics.

The present investigation was undertaken as a first step in the development of a proposed technique for obtaining quantitative information about the flow field. This proposed technique involves the study of the vorticity distribution in the wake with the initial emphasis being directed toward the trailing-vortex system shed from the blade tips. Unlike the case of the three-dimensional wing, in which the induced motion of the trailing-vortex system normal to the flight path may be neglected, the induced motion becomes very important in hovering and low-speed forward flight of the helicopter rotor. This induced motion must be determined within a reasonable degree of accuracy if the classical vortex theory is to yield good results for the induced velocity components throughout the field and particularly at the blade feathering axis. The theoretical determination of the motion is possible but is exceedingly laborious. An experimental technique was developed in references 2 and 3 in which smoke was injected into the tip vortex and the resulting tip-vortex pattern was photographed. The position of the tip vortex could be easily determined but the determination of the velocity components required a time-consuming numerical integration of the Biot-Savart equation. Reference 4 presents an electromagnetic analog for determining the induced velocity for the entire field of a uniformly loaded lifting rotor in which the wake was replaced by the electrical analog of a uniform vortex cylinder, namely, a closely spaced wire coil. This was shown to be a relatively fast, accurate means of determining the velocity components but was restricted to the ideal cases since no information was available for constructing wire models of actual wake-vortex patterns. It therefore appeared that

a very useful experimental procedure would be obtained by combining the smoke technique which yielded the vortex pattern with the electromagnetic analog from which the velocity field could be easily determined by measurement. It is this method and its results that are presented in this report for the case of hovering and steady low-speed flight within ground effect.

This investigation was conducted at the Georgia Institute of Technology under the sponsorship and with the financial assistance of the National Advisory Committee for Aeronautics.

SYMBOLS

B	magnetic flux density
B_N	magnetic flux density at center of reference coil carrying current I
B_P	magnetic flux density at point P of wire model
b	number of blades
C_T	rotor thrust coefficient, $\frac{T}{\rho\pi R^2(\Omega R)^2}$
C_Γ	tip-vortex strength coefficient, $\frac{\Gamma}{4\pi R^2\Omega}$
ds	length of vortex element
ds'	length of current-carrying element of wire model
I	current flowing through wire model and reference coil
n	number of turns of wire on reference coil
R	rotor radius
R_c	radius of reference coil
R_m	wire-model rotor radius
r	radial distance from Z-axis (rotor axis)
r'	distance from point P to element ds of vortex

r_m distance from point P to element ds' of wire model

T rotor thrust

V velocity along flight path

V_i' induced velocity associated with tip vortex

V_{i_N}' induced velocity at center of vortex ring of strength Γ

V_{i_P}' induced velocity at point P of rotor

w component of induced velocity that is associated with tip vortex and is normal to rotor plane

$\bar{w}$ mean value of normal component of induced velocity w

Z vertical distance from rotor plane, positive in a downward direction

β angle between extension of line joining point P with element ds of vortex and plane normal to element

β' angle between extension of line joining point P with element ds' of wire model and plane normal to element

Γ tip-vortex strength

μ advance ratio, $\frac{V}{\Omega R}$

$\bar{\mu}$ permeability of medium surrounding wire model and coil ($\bar{\mu} = 1.00$ for air)

ρ mass density of air

ψ azimuth angle of blade feathering axis measured from downwind position and in direction of blade rotation

Ω rotor angular velocity

APPARATUS

Model Rotor

The 4-foot-diameter model was a two-blade, teetering type with no coning or lag angles. The blades had an NACA 43015 airfoil section, a square tip with a chord of 1.508 inches, a taper ratio of 2 to 1, and a solidity ratio of 0.05. The airfoil section of the blades began at a point 4.5 inches from the axis of rotation and had a steel leading edge and a laminated walnut trailing edge. The blade collective pitch angle could be manually set within a range of 0° to 10°.

Buried within the walnut trailing edge and running the length of each blade was a thin-wall, 0.10-inch-outside-diameter, stainless-steel tube which conducted the smoke-producing agent, liquid titanium tetrachloride, through the blade to the cotton-filled smoke generator at the blade tip. Each smoke generator was made of a 1/2-inch length of 3/16-inch-outside-diameter stainless-steel rod, drilled 5/32 inch through and perforated with 1/32-inch holes. The generator was silver-soldered to the tube in a position midway along and parallel to the blade-tip chord line. The tube was connected by a length of polyethylene tubing to the reservoir which was mounted on the drive shaft.

Rotor Test Stand

The rotor test stand consisted of a base plate upon which the drive motor and drive shaft support were mounted with their axes vertical as in figures 1 and 2. The shaft support housing was a 4-inch-outside-diameter flanged pipe, 35 inches long. Within this outer pipe were two concentric drive shafts. The outer drive shaft was mounted on ball bearings and was driven by a timing belt drive at its upper end. The inner shaft was driven through a ball-bearing slip and universal joint inside and at the upper end of the outer shaft. The inner drive shaft was centered by an aluminum-alloy diaphragm near its lower end, and was restrained from vertical movement by a strain-gage beam fixed to the shaft support housing and connected to the diaphragm bearing assembly. This strain-gage beam measured the thrust of the rotor. The rotor itself was mounted on the lower end of the inner drive shaft.

The rotor was driven by a 1/2-horsepower, 24-volt direct-current aircraft motor which was supported by ball bearings on its output shaft. The motor was prevented from rotating by a strain-gage beam in simple bending which measured the torque. The motor speed was changed by varying the armature current which allowed a realizable range of rotor speeds of 0 to about 700 rpm with blades set at the test collective pitch angle.

The rotor thrust stand was mounted at the desired height on a carriage which ran on tracks suspended from the ceiling of the test room as shown in figure 3. Hence the area underneath the rotor was completely free of obstructions. The carriage was cable-driven by a variable-speed reversible motor and had about 28 feet of travel.

Photograph Equipment

The smoke pictures were taken by two shutterless, 35-millimeter-oscillograph-recorder-type cameras mounted on the carriage. When the cameras were operating, the test area was unlighted except for a stroboflash unit which was triggered every 210° of rotation of the rotor by a commutator on the outer drive shaft. This 210° represented the recharge time of the stroboflash at a rotor speed of about 600 rpm. Thus seven turns of the rotor were required to obtain a complete set of pictures at 30° intervals. The light source was placed above and behind the wake with respect to the cameras and had a flash duration of about 30 microseconds.

Test Site

The test site was a room $41\frac{3}{4}$ feet long by $16\frac{1}{4}$ feet wide by 11 feet high. Although a wide-angle lens was used in the cameras, it was necessary to offset the model track from the centerline of the room in order that the rotor wake would fall in the camera field of view. This compromise placed the retreating blade tip about $3\frac{1}{2}$ feet from the wall.

Instrumentation

As mentioned before, the thrust and torque were measured by strain-gage beams in simple bending. The signal was carrier amplified and then recorded by an oscillograph recorder. The calibration curve was obtained by loading both beams with known weights whose values were plotted versus the measured deflection of the galvanometer trace from the zero reference.

The rotor rpm were determined by counting the recording oscillograph galvanometer trace deflections caused by an electrical pulse introduced into the circuit by a commutator mounted on the outer rotor drive shaft. The forward speed was determined by counting the recorded revolutions of a synchronous generator which was driven by the carriage drive cable. The time standard for both of these measurements was 60-cycle commercial power-line frequency which was also recorded by the oscillograph.

Electromagnetic Models

The electromagnetic models were constructed from the data obtained from a study of the smoke pictures from which the intersections of the tip vortices with the 45° interval planes perpendicular to the rotor disk plane were determined. The wire supports were made from fiber board and were mounted on a glued-up plywood base as shown in figure 4. Copper wire, No. 17 gage, was used and was wrapped upon the model supports at the tip-vortex position for the blades at given azimuth angle. Four complete turns of the vortex helix were simulated. Since the induced velocity component w normal to the rotor disk was the only one to be measured, the lead wires were positioned in the plane determined by the blade feathering axis and the search-coil axis so that they were either parallel or perpendicular to the axis of the search coil. In these positions, there should be no contribution of the lead-in wires to the field measurements since all the measurements were made in this same plane at the simulated blade feathering axis.

The three wire models for advance ratios $\frac{V}{\Omega R}$ of 0, 0.022, and 0.030 $\left(\text{or } \frac{V}{\Omega R\sqrt{\frac{1}{2} C_T}} \approx 0, 0.48, \text{ and } 0.65\right)$ are shown in figures 4(a), 4(b), and 4(c), respectively. In order to simplify the models, the vortex from only one blade was simulated. The result for two blades was obtained by superimposing the measurements taken with the wire model of the tip vortex displaced 180° in azimuth on the wire supports.

Electromagnetic Analog Apparatus

The electromagnetic analog apparatus was essentially the same as that described in reference 4 except that the 400-cycle generator was driven by a synchronous motor.

TEST PROCEDURE

Prior to the tests, the rotor was hovered out of ground effect and the blade angles were differentially adjusted until the rotor tips tracked. Once the tips tracked, the collective pitch angle of the blades was reduced until a smoke probe showed that zero thrust had been reached. Knowing the various lever arms and screw thread pitches in the manual collective-pitch adjustment links, the blade-pitch change was calculated per turn of the adjustment links and the blades were set at an effective angle of 7.2°. All tests were run at this blade-pitch angle.

With the rotor hovering out of ground effect, smoke was introduced into the tip vortices of both blades and the resulting patterns were photographed and compared. Since they were identical within the accuracy of the present measurements, it was decided to introduce smoke into only one of the blade-tip vortices for the remainder of the tests because the smoke filaments tended to obscure one another in the photographs. The rotor test stand was then lowered until the rotor disk was 1 rotor radius above the floor and the testing was begun.

With cameras and oscillograph recorder on standby, the smoke generators were checked. If the smoke was satisfactory, the rotor was quickly brought to speed and the carriage was started. When the model had reached a steady forward speed the room lights were turned off and the stroboflash unit, the cameras, and the oscillograph recorders were turned on. After the data were obtained, the recording equipment was turned off and the carriage and rotor were stopped. This completed a single run.

Only one ground height could be tested within the scope of this investigation and this height was chosen to be 1 rotor radius. Inasmuch as it was not possible to view the vortex pattern while the model was in motion, it was necessary that a series of runs be made at various forward speeds in order to bracket the tuck-under point. This point was then determined from a frame-by-frame study of the smoke pictures. All data were taken in steady-state conditions.

The photographs were studied for each run and the tip-vortex positions on the longitudinal and lateral boundaries of the wake were determined at 30° intervals of blade rotation. From these data, the electromagnetic models were constructed and the field strength measurements were taken, as mentioned before, across the diameter defined by the blade feathering axis using the procedure of reference 4. Since only one tip vortex was simulated by the model at a time, eight different wire models were used for each run in order to cover the disk at 45° intervals. Changing from one blade azimuth position to the next merely involved changing the wire position on the wake boundary model and could be very quickly accomplished.

The effect of the ground plane was determined by the method of images except that the same model was used as the image as will be explained more fully later. Measurements were made across the diameter and parallel to the blade feathering axis at a distance of 2 rotor radii beneath the simulated rotor disk plane.

REDUCTION OF DATA

The initial thrust and torque strain-gage oscillograph traces contained such a high "noise" level that no reliable data could be obtained.

A resistor-capacitor filter which virtually eliminated all of the rotor harmonic content of these traces was then placed in the circuit. Upon testing these revised circuits a drift of the zero reference was observed in both channels. A considerable amount of time and effort was spent in trying to eliminate this drift, but its source could not be determined. Consequently the strain-gage data are not included in the report.

The accuracy of the rotor rpm and flight-velocity measurements is a direct function of the number of turns involved and the accuracy with which the time standard could be read from the record. It is estimated that the time could be determined within ±0.002 second. The maximum error in rpm is thus about ±1.2 rpm and in velocity, about ±0.005 foot per second.

To obtain the tip-vortex position in the longitudinal and lateral planes of the wake as a function of blade azimuth position, each picture was projected on an 11- by 17-inch sheet of graph paper at a scale of 1 to 4.8 so that the result was a nondimensional plot of r/R versus Z/R. The data were then corrected for camera perspective, the points were plotted versus blade azimuth position, and a curve was drawn through the points. Although there is a maximum error of about ±1 inch in determining the position of the tip vortex, it is felt that the faired data are a close representation of the vortex position. The faired curves were then used in the construction of the electromagnetic analogs.

It was not possible to locate the tip-vortex position any closer to the ground plane than about $0.25R$ to $0.4R$, which meant that only about two turns of the vortex helix could be obtained from the photographs. As will be discussed later, it was decided to extrapolate the data by calculating the motion of an isolated vortex ring whose axis was normal to a ground plane. Two additional turns were obtained in this manner, making a total of four turns of the vortex helix for each model.

The meter readings were referenced or normalized to the magnetic field strength at the center of an isolated wire coil consisting of nine closely spaced turns of wire wrapped on a Plexiglas ring. This coil was in series with the wire model and was used because the field strength could be calculated from the measured quantities and the calibration factor for the complete analog could thus be easily obtained.

For purposes of making the measurements, the current flowing in the wire model and the reference coil is completely arbitrary. However, to convert the measured ratios to meaningful values for the velocity field, a conversion factor must be determined since it is the value of the vortex strength coefficient C_Γ which largely determines the geometry of the tip-vortex pattern when $V \ll V_i'$. Here, by definition

the diameter of the wire model corresponding to the blade feathering axis. The wire model was next displaced 1 rotor diameter along the rotor axis and then was rotated about the feathering axis. A survey was made along the same spatial line (i.e., a line parallel to but now two rotor radii below the wire model diameter corresponding to the blade feathering axis) with the original wire model now acting as the image. (Note that this does not give a true mirror image, but one in which the wire simulating the tip vortex is wound in the opposite direction to the true image. The measurements for the normal component, however, are the same in either case.) The resultant normal component is found by taking the difference of these two measurements. An advantage is realized by this approach in that the effects of all stray magnetic fields tend to be cancelled. The wire was then wrapped on the wire model supports for the tip vortex starting from the $\psi = 180^\circ$ blade-tip position and the same procedure was repeated. The sum of the two results is then the normal component of induced velocity that is associated with the tip vortices of a two-blade rotor in low-speed forward flight with the blades in the 0° to 180° position. An example is given in figure 5, which shows the measurements made for each of the four surveys and their resultant for the 0° to 180° plane and for $\mu = 0.022$ or $V/\Omega R\sqrt{\frac{1}{2} C_T} \approx 0.48$. It is to be noted that neither survey by itself is useful or corresponds to the tip-vortex pattern of a single blade since the vortex pattern of a single blade is appreciably different.

TEST RESULTS

The results of the smoke study are presented in figures 6 and 7. These figures give the paths of the tip vortex and the positions along these paths at 90° intervals of blade rotation for various advance ratios and azimuth cutting planes. Figure 6 shows the change in the longitudinal cross section as a function of the advance ratio. From this figure it can be seen that the downwind paths do not experience as large a variation in position as do the upwind paths for $\mu > 0.011$ with the main change occurring at the tuck-under point. For the upwind paths, the $\psi = 180^\circ$ azimuth planes, the changes in position appear to occur relatively smoothly with again the largest rate of change occurring near the tuck-under point. There are some exceptions to these generalities, in particular for $\mu = 0.013$ and 0.018 at the downwind side. For the case of $\mu = 0.037$ at $\psi = 180^\circ$, the smoke study definitely shows an oscillation in the vortex path with a vertical amplitude of about 5 inches at subrotor frequency. The path shown is the mean for this case. It may be that these three cases represent nonsteady conditions.

The three cases that were completely analyzed were for $\mu = 0$, 0.022, and 0.030 $\left(\text{or } V/\Omega R\sqrt{\frac{1}{2} C_T} \approx 0, 0.48, \text{ and } 0.65, \text{ respectively}\right)$ since it appeared that the wake tuck under occurred between the latter two runs. The cross sections of the tip-vortex paths for the 0° to 180°, 45° to 225°, 90° to 270°, and 135° to 315° azimuth planes for $\mu = 0.022$ and $\mu = 0.030$ are shown in figure 7 along with the hovering cross section for comparison purposes. The location of the tip vortex at 90° intervals of blade rotation is also shown. The broken lines indicate the extrapolated tip-vortex paths. It is noted that the measured portion of the wake boundary appears to be symmetrical about the longitudinal plane prior to tuck under. It is also noted that the wake axis is inclined at a greater angle to the vertical in low-speed forward flight within ground effect than out of ground effect when compared with the data of references 3 and 6.

W
1
4
3

The nondimensional normal component of induced velocity that was associated with the tip vortex and was determined from the electromagnetic analog for the blade feathering axis is shown in figure 8 for $\mu = 0.022$ and $\mu = 0.030$, respectively, with the hovering distribution included in the figure for comparison purposes. As can be seen, the greatest change in induced-velocity distribution from hovering occurs close to the blade tips and is a direct result of the changes in vortex pattern due to forward flight. This may be seen, particularly for the longitudinal plane, by correlating the induced-velocity distributions of this figure with the vortex positions of figure 7.

The mean effective values of the nondimensional induced velocity at the blade feathering axis and associated with the tip vortex were determined and are also plotted in figure 8. These values are $(\bar{w}R/\Gamma) = 1.830$ and 1.562 for $\mu = 0.022$ and 0.030 $\left(\text{or } V/\Omega R\sqrt{\frac{1}{2} C_T} \approx 0.48 \text{ and } 0.65\right)$, respectively. For hovering flight, $\bar{w}R/\Gamma = 1.958$. Thus there is a reduction in the normal mean effective induced velocity from hovering to $\mu = 0.030$ of about 20 percent with 13.5 percent of this reduction occurring in the last 0.008 change in advance ratio.

DISCUSSION OF RESULTS

As was mentioned before, it was not possible to determine the position of more than two turns of the tip vortex from the photographs. The disappearance of the smoke was rather sudden and was analogous to that reported in reference 3 in which the photographs showed that, under certain conditions, the smoke in the tip vortex from a single isolated blade split at the leading edge of the wake and thereafter appeared to diffuse or dissolve, beginning at the longitudinal plane and extending

downwind azimuthally in both directions with time. The difference for the case within ground effect was that the diffusion was independent of flight direction and in all cases occurred at about the same height off the ground. It did not appear to be reasonable that the velocity field associated with the vortex elements beyond the point at which the smoke trace vanished would also vanish since there were no external forces in evidence. On the other hand, the effect of viscosity enlarges the core of a line vortex. This fact in itself could result in a diminishing of the smoke density. However, viscous fluid theory for a line vortex indicated that the growth of the vortex core would be relatively slow while the region outside this rotational core remained essentially potential. Therefore, as far as the blade feathering axis was concerned, the vortex field would appear to remain potential.

Assuming the above to be true, the next step is to determine the motion of the vortex after it could no longer be photographed. It was decided that certainly the simplest configuration would be the most desirable at this stage and the decision was made to extrapolate the motion of the tip vortex by assuming it to be the same as the motion of a vortex ring as it approached a ground plane along its axis. In order to match the helical vortex path in hovering flight with the ring-vortex path, the strength of the ring vortex was adjusted until the velocity vector of an element of the ring was identical with that of the last element photographed. The result of this extrapolation is shown in figure 7(a) as a broken line.

This extrapolation is in error on at least two counts. First, the ring-vortex strength must be fictitiously high to match the motion of the helical vortex at the last point photographed so that as the ring approaches the ground plane its radial velocity will be too large. Second, as the helical vortex approaches the ground and as the effects associated with the rest of the vortex field become small compared with those of the adjacent elements of the image, the apparent radial motion of the helical vortex will be higher than the actual radial velocity of the fluid in the vortex core because of the presence of a tangential velocity at the core. As the angle between the helix and the radial coordinate lines becomes smaller and smaller as the helix approaches the ground plane, the motion of the helix elements becomes largely tangential and the helix will tend to unwrap. These two effects are in opposite directions so that the errors will tend to cancel.

The results of this extrapolation for hovering flight are shown in figure 9. Curve A of this figure is the nondimensional normal component of induced velocity that is associated with the first two turns of the tip vortex, that is, the portion of the tip vortex that could be photographed. Curve B shows the results of adding two more turns according to the previous discussion. Curve C shows the results of adding three arbitrary turns of constant radial spacing but using the same wake

boundary as for curve B. The length of the wire in the electromagnetic models was the same for both B and C. It is felt that curve B more nearly represents the true picture than either of the other curves.

For $\mu = 0.022$ $\left(\text{or } V/\Omega R\sqrt{\frac{1}{2} C_T} \approx 0.48\right)$, there was no question about the wake spreading in all directions since the smoke pictures of the tip vortex showed this to be true as shown in figure 7(a). The wake was then extrapolated for two additional turns in a manner similar to that in hovering flight.

For $\mu = 0.030$ $\left(\text{or } V/\Omega R\sqrt{\frac{1}{2} C_T} \approx 0.65\right)$, the smoke pictures did not show the spreading at the leading edge of the wake, and since there was a relatively large change in the vortex pattern, it was assumed that the wake had tucked under. When the time came to construct the electromagnetic wire model, however, the problem arose as to how the tip-vortex path should be extrapolated since the upstream elements of an isolated vortex ring in a uniform potential flow parallel to a ground plane will always, at some ground height, begin to move upstream.

In order to gain some insight into this phenomenon, some additional tests were run. Smoke generators were placed down the length of the room at intervals of 1 diameter along a radial line through the rotor axis and several inches above the ground plane. The rotor was brought up to speed in hovering flight as quickly as possible and the time required for the wake to reach the region in which the forward flight pictures were made was determined. This region began 4 diameters from the starting point and the time required for the wake to reach this point was about 12 seconds from the time the rotor reached full rpm or about 16 seconds from start. The time was determined by stopwatch and was an average over several runs. With the carriage at the starting point, the rotor was again brought up to speed as quickly as possible. When full rpm was reached, the carriage was started. From an average of several of these runs, it was determined that the wake reached the 4-diameter point about 9 seconds after the carriage was started or in about 3 seconds less than that required for the wake of the rotor in hovering flight. Further tests showed that the wake several inches above ground level was about 1 rotor radius ahead of the leading edge of the rotor. It therefore appears that the wake is not truly tucked under for $\mu = 0.030$. In the light of these tests, the tip-vortex path was again extrapolated in a manner similar to the former. The wire model is shown in figure 4(c).

In order to determine the effect of forward velocity, other runs were made. It was found that increasing μ reduced the distance that the wake was out in front of the rotor but did not appreciably change

the tip-vortex path in the immediate vicinity of the rotor as shown in figure 5. Consequently, it is believed that the major changes in flight attitude would probably occur between $\mu = 0.022$ and 0.030 $\left(\text{or } V/\Omega R \sqrt{\frac{1}{2} C_T} \approx 0.48 \text{ and } 0.65, \text{ respectively}\right)$ for the model rotor. This is borne out to some extent by the fact that is was shown previously in the test results that there was a relatively large reduction in mean normal component of tip-vortex-induced velocity in this range of advance ratios.

An unexpected flow phenomenon was observed during these qualitative tests in hovering flight. For several seconds, the smoke streamers would indicate a relatively steady flow largely in a radial direction but with a tangential component in the same direction as the blade rotation. Then a disturbance would occur at the innermost smoke generator which would cause the streamer to fluctuate in direction. This disturbance would move radially and was observed out to the fifth-diameter station. The propagation velocity did not appear to be uniform although the disturbance did appear to reoccur every 2 or 3 seconds under the test conditions. Additional smoke probes were placed beneath the rotor tips and the disturbance was again observed. The disturbance appeared to be a rolling up and then the shedding of a vortex system from the region near the ground plane beneath the rotor. This disturbance appeared to be similar in both nature and origin to that shown in the motion-picture film supplement of reference 7 except for the occurrence at a greater ground height.

As was mentioned before, the tip-vortex path was unsteady at an azimuth position $\psi = 180^\circ$ and $\mu = 0.037$. Reference 1 shows that the maximum vibratory blade bending and torsional moments during a low-speed approach occur at $\mu \approx 0.047$ with the maximum rate of increase appearing to occur at $\mu \approx 0.031$. It was pointed out in this reference that the increased moments were felt to be the result of the rapidly changing flow characteristics through the rotor. This contention is therefore given concrete support by the observations made during this particular case. However, a run was also made at $\mu = 0.0350$ during which this unsteadiness was not observed. The criteria for this steady or unsteady motion of the tip vortex were not determined.

It is felt that, in general, the approach presented in this report is well suited to the investigation of low-speed vortex systems. The most time-consuming part of the procedure was the step between the smoke pictures and the electromagnetic model. Once the equipment was operating, the smoke pictures could be obtained very quickly. Likewise, after the electromagnetic wire supports had been designed, the survey across the blade feathering axis could be completed quickly and accurately and the change to a different blade azimuth position could be accomplished easily. Some time was spent trying to bridge this gap by projecting

the pictures back together and attempting to trace the tip vortex out in space. It became evident, however, that considerable development time and some special equipment would be required so this approach was dropped. It is recommended that this or some similar technique be developed or adopted if any further work along these lines is done.

The author of reference 8 reports that an attempt was made to determine the streamlines about a lifting rotor that was hovering within ground effect by using an approach similar to that of reference 8. However, in order to satisfy the boundary conditions, an anomaly arose which required that the radial velocity of the elements of the uniform vortex cylinder had to approach infinity and the sheet strength had to approach zero as the wake-vortex sheet approached the ground plane. In the actual case this anomaly never arises even in a potential flow because the adjustment can take plane in the vortex spacing; that is, the mean induced velocity can go to zero while the vortex motion remains finite and the strength also remains finite. It is believed that in a potential flow the tip vortex would eventually become radial since it starts out as a spiral and, as it approaches the ground plane, the effect of the image is to increase the tangential motion and hence to incline the vortex more nearly parallel to the radial coordinate lines. This would result in an infinite spacing at infinity, a zero mean radial velocity, and a finite tangential velocity of the vortex. In a real flow, the action of viscosity increases the vortex core diameter (i.e., the rotational portion of the vortex system) and it would appear that the presence of the ground plane would break up the vortex relatively quickly when the core radius becomes of the same order of magnitude as its height above the ground plane.

Finally, it is to be noted that the induced-velocity distributions presented are those due to the tip vortex of this particular model rotor. It is believed that they may be used with good accuracy for other two-bladed rotors, but the flow field for single-blade rotors is certainly appreciably different and the flow field for rotors of three or more blades may also be appreciably different.

CONCLUDING REMARKS

The primary purpose of this investigation was the development of the technique of using electromagnetic analogs to determine the velocity field due to a vortex pattern obtained from experimental smoke-flow studies of the wake of a model helicopter rotor operating within ground effect. It is concluded that the method herein presented is well-suited to the study of periodic vortex patterns and that measurements of engineering accuracy were obtained.

Several phenomena were observed which are believed to be worthy of further investigation. One was the inability to photograph more than about two turns of the tip-vortex helix. What happens to the vortex beyond this point has an appreciable effect on the normal component of induced velocity at the blade feathering axis. The second phenomenon was an apparent rolling up and subsequent shedding of a vortex system from the region near the ground plane and underneath the rotor at sub-rotor frequencies. The cause of this disturbance, whose effects were observed out to 5 rotor diameters is unknown, but its origin and nature appeared to be much the same as those noted in reference 7.

Inasmuch as it was not possible to photograph the smoke patterns close to the ground plane, the actual tuck-under point was taken at that advance ratio at which the greatest change in tip-vortex position was observed. For this model and a ground height of 1 rotor radius, it occurred between $\mu = 0.022$ and 0.030 $\left(\text{or at } V/\Omega R\sqrt{\frac{1}{2} C_T} \approx 0.48 \text{ and } 0.65, \text{ respectively}\right)$. There also occurred between these two runs a $13\frac{1}{2}$-percent reduction in the mean effective, tip-vortex induced velocity.

Georgia Institute of Technology,
Atlanta, Georgia, August 1959.

REFERENCES

1. Ludi, LeRoy H.: Flight Investigation of Effects of Transition, Landing Approaches, Partial-Power Vertical Descents, and Droop-Stop Pounding on the Bending and Torsional Moments Encountered by a Helicopter Rotor Blade. NASA MEMO 5-7-59L, 1959.

2. Gray, Robin B.: On the Motion of the Helical Vortex Shed From a Single-Bladed Hovering Model Helicopter Rotor and its Application to the Calculation of the Spanwise Aerodynamic Loading. Rep. No. 313, Princeton Univ. Aero. Eng. Dept., Sept. 1955.

3. Gray, Robin B.: An Aerodynamic Analysis of a Single-Bladed Rotor in Hovering and Low-Speed Forward Flight as Determined from Smoke Studies of the Vorticity Distribution in the Wake. Rep. No. 356, Princeton Univ. Aero. Eng. Dept., Sept. 1956.

4. Castles, Walter, Jr., Durham, Howard L., and Kevorkain, Jirair: Normal Component of Induced Velocity for Entire Field of a Uniformly Loaded Lifting Rotor With Highly Swept Wake as Determined by Electromagnetic Analog. NASA Tech. Rep. R-41, 1959. (Supersedes NACA TN 4238.)

5. Castles, Walter, Jr., and New, Noah C.: A Blade-Element Analysis for Lifting Rotors That Is Applicable for Large Inflow and Blade Angles and Any Reasonable Blade Geometry. NACA TN 2656, 1952.

6. Gessow, Alfred: Review of Information on Induced Flow of a Lifting Rotor. NACA TN 3238, 1954.

7. Heyson, Harry H.: An Evaluation of Linearized Vortex Theory as Applied to Single and Multiple Rotors Hovering In and Out of Ground Effect. NASA TN D-43, 1959.

8. Castles, Walter, Jr.: Approximate Solution for Streamlines About a Lifting Rotor Having Uniform Loading and Operating in Hovering or Low-Speed Vertical-Ascent Flight Conditions. NACA TN 3921, 1957.

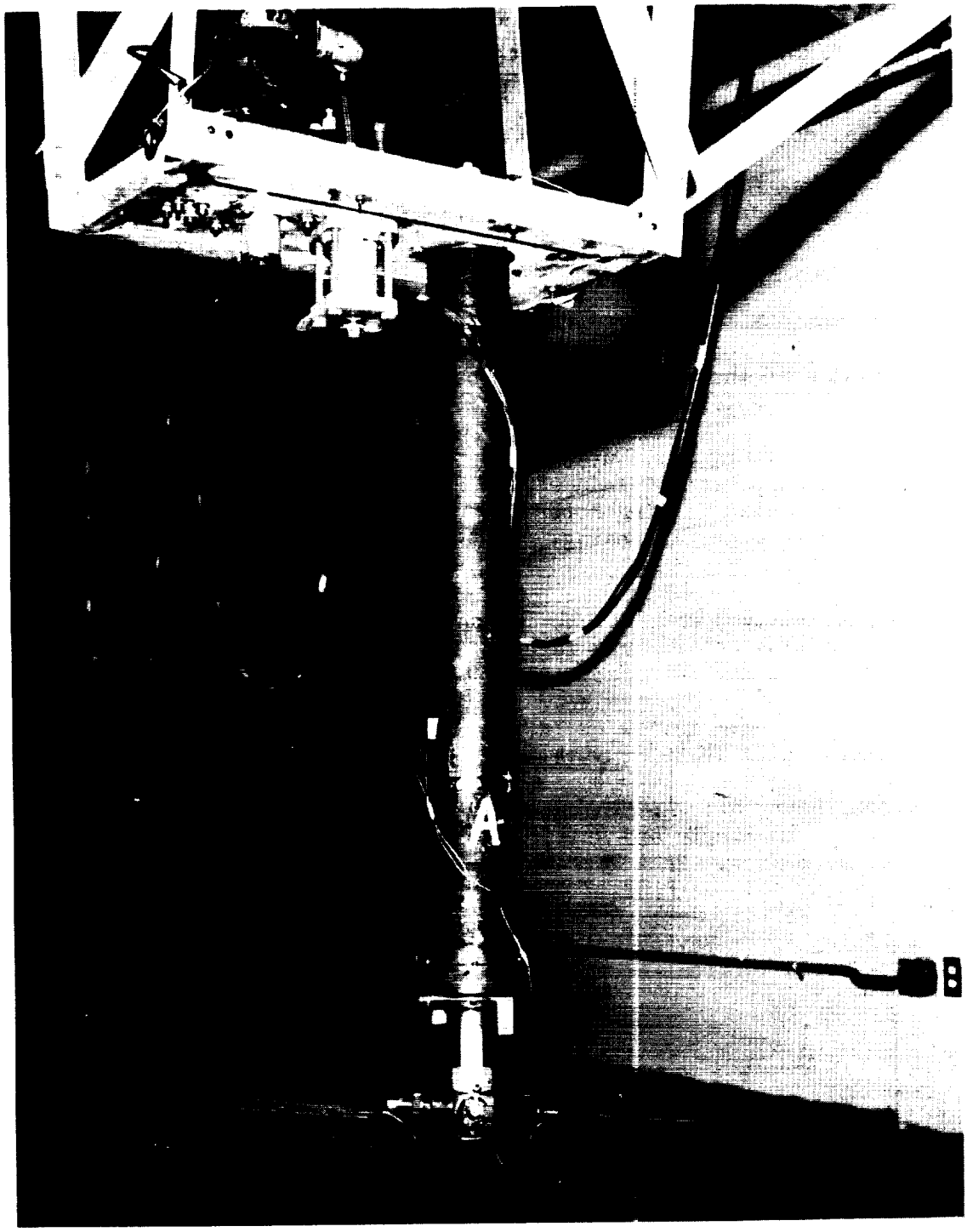

Figure 1.- Model rotor test stand. L-60-288

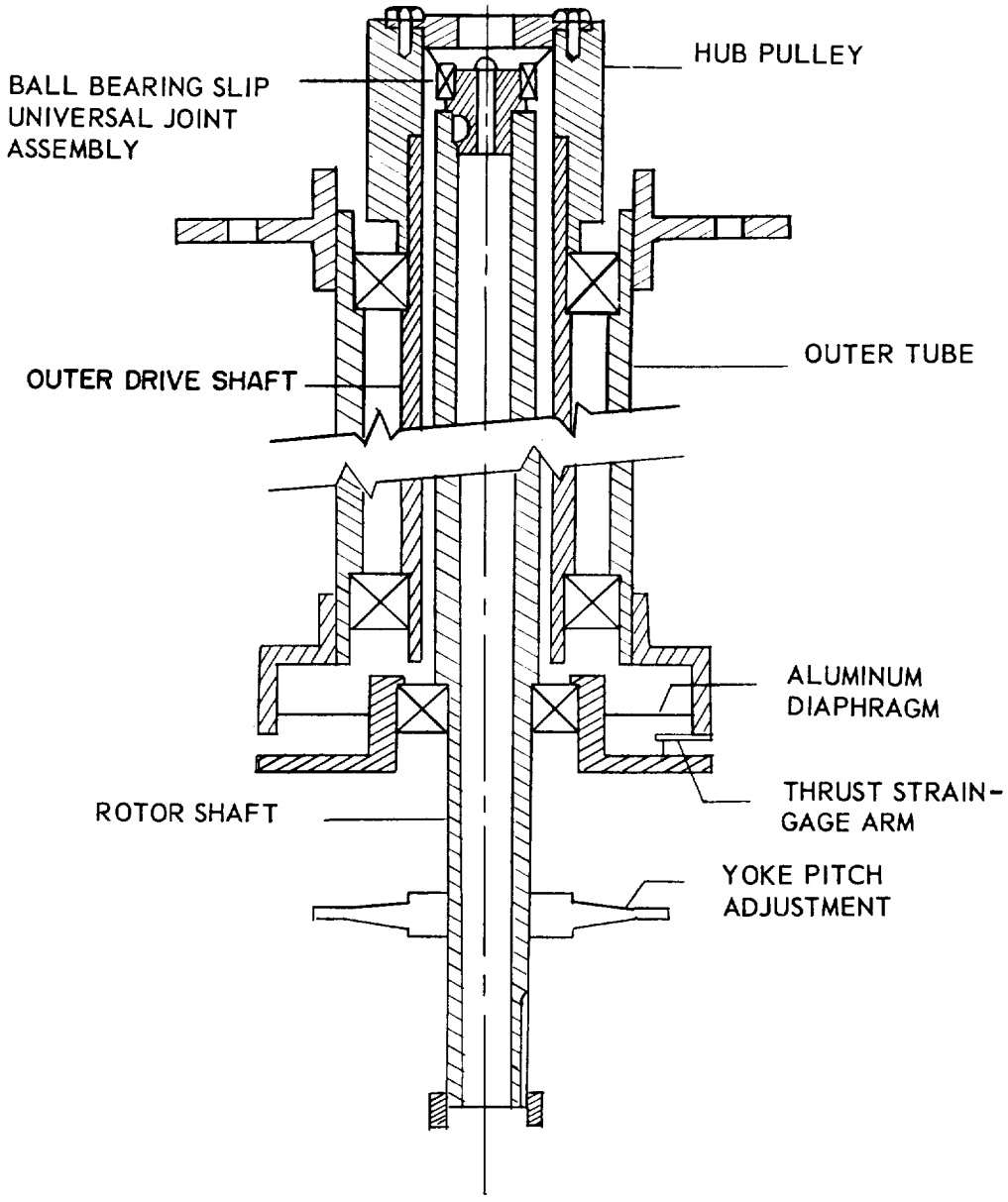

Figure 2.- Schematic drawing of rotor test stand. Drawing is to half scale.

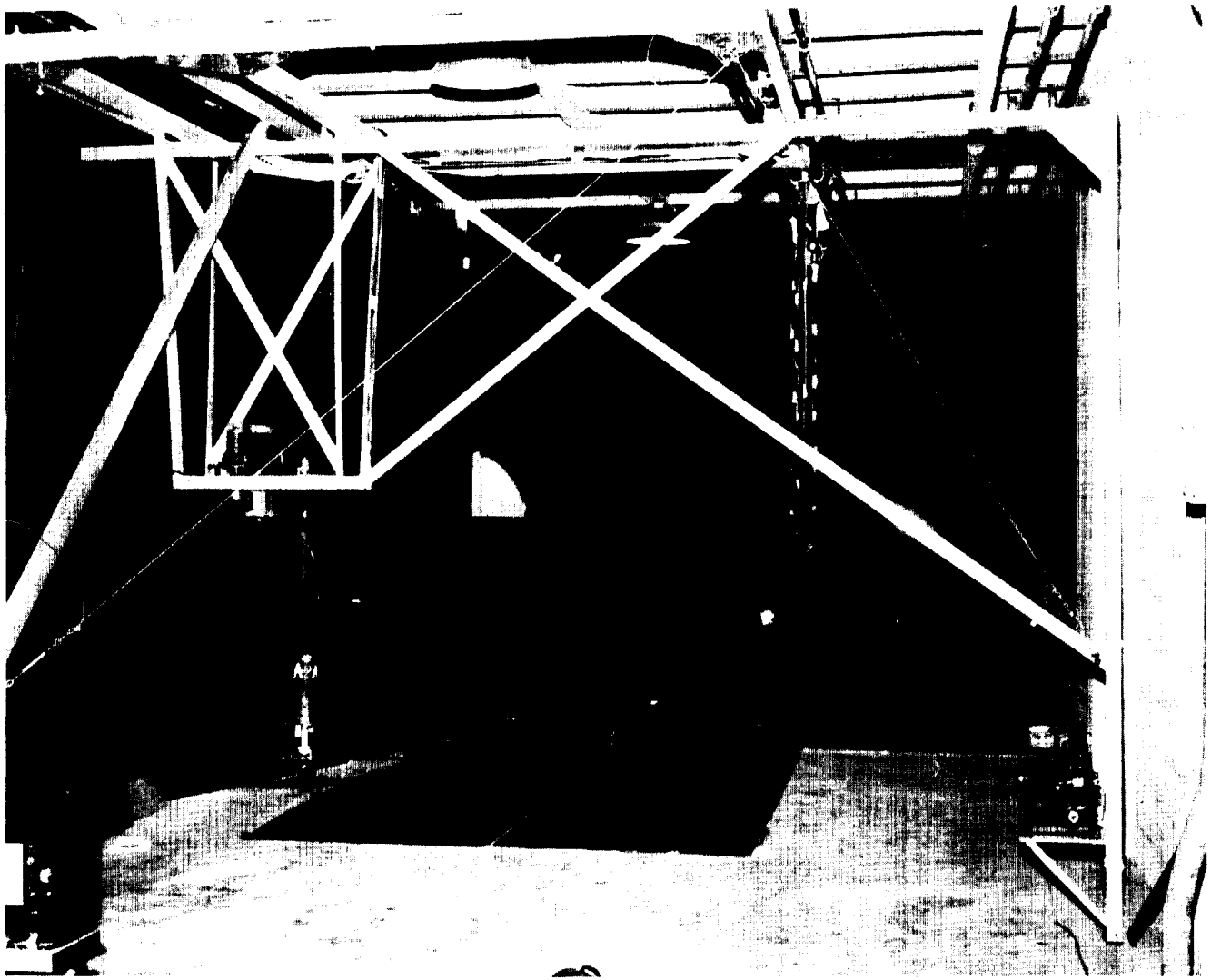

L-60-289

Figure 3.- Rotor test stand and support carriage showing camera position.

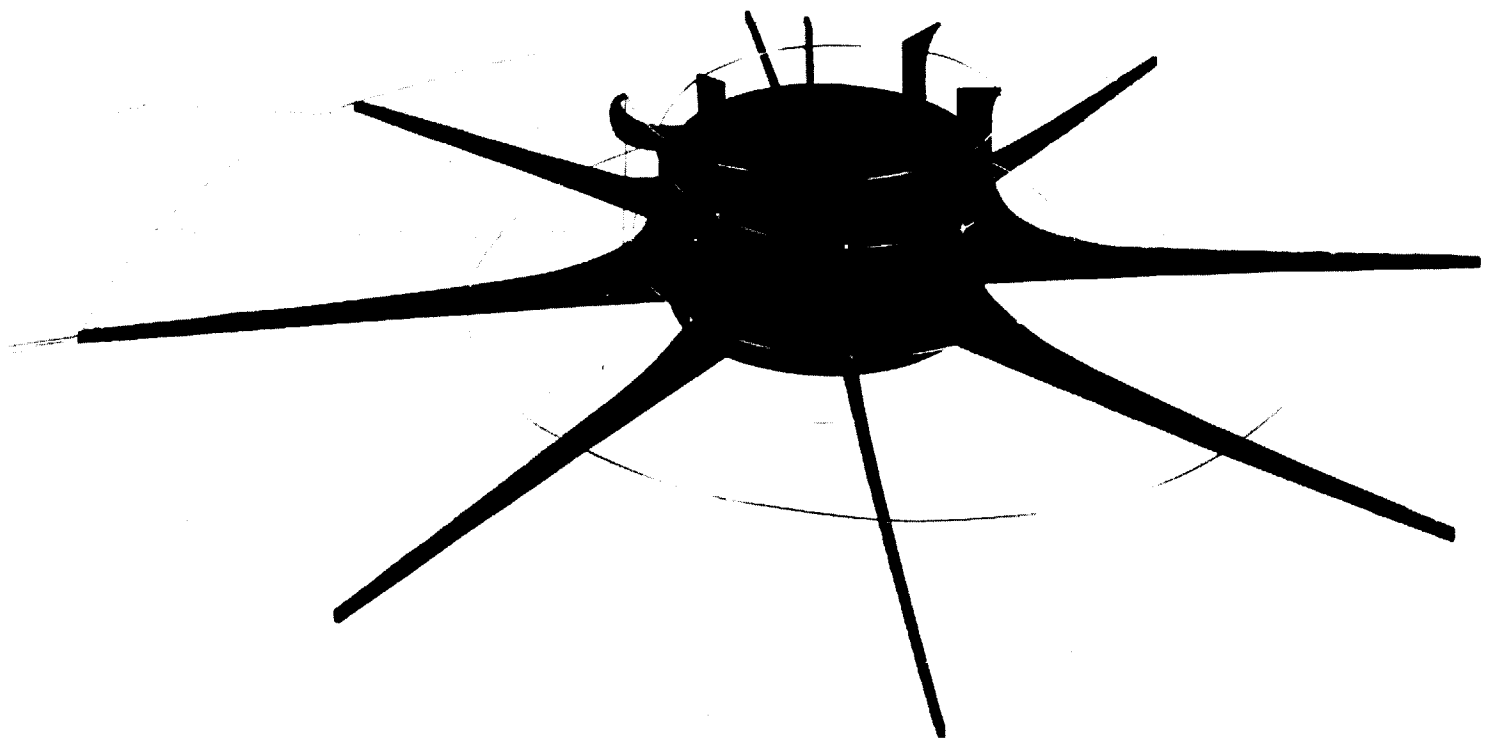

(a) Hovering case; $\mu = 0$.

L-60-290

Figure 4.- Electromagnetic analog of tip vortex of a two-blade model rotor showing only one of tip-vortex systems.

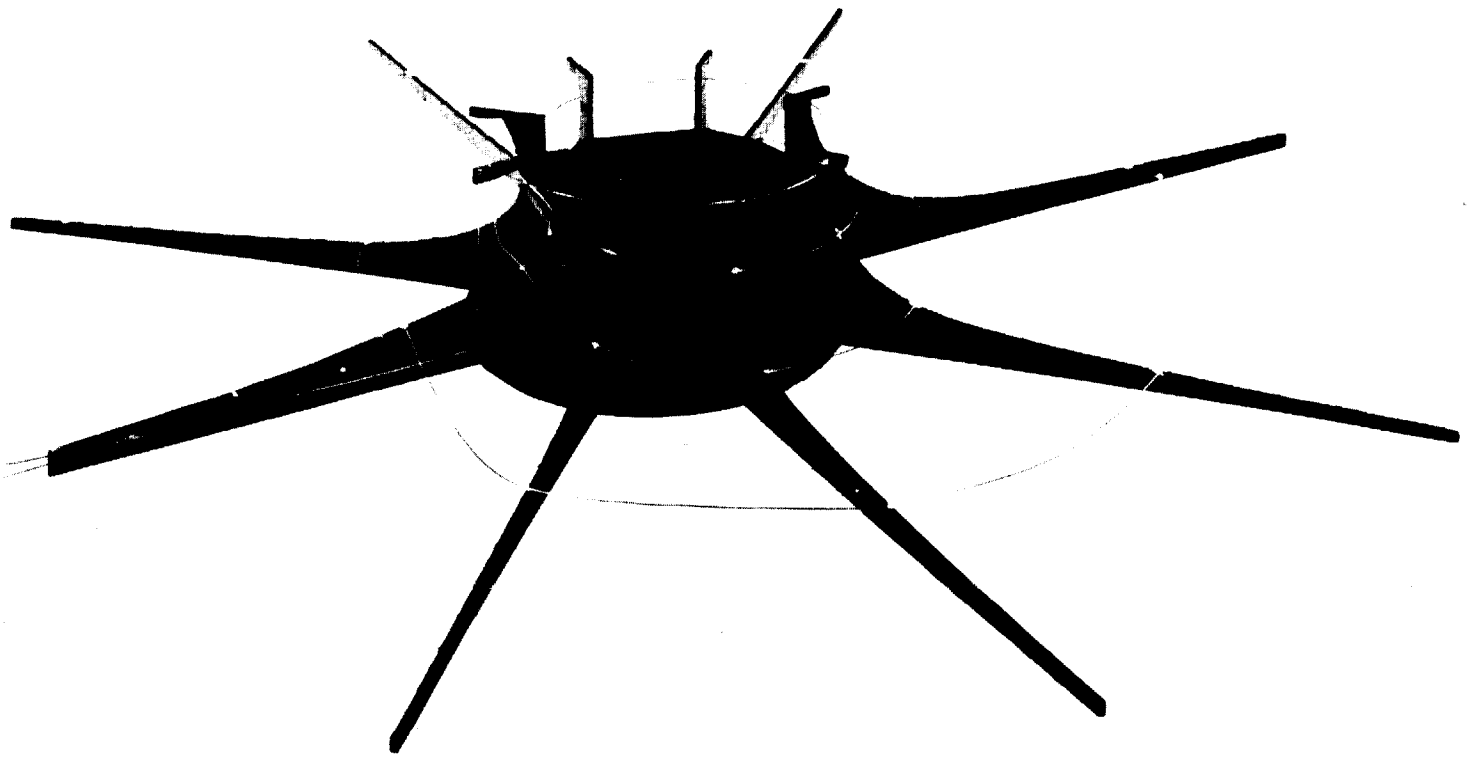

(b) $\mu = 0.022; \frac{V}{\Omega R\sqrt{\frac{1}{2} C_T}} \approx 0.48.$ L-60-291

Figure 4.- Continued.

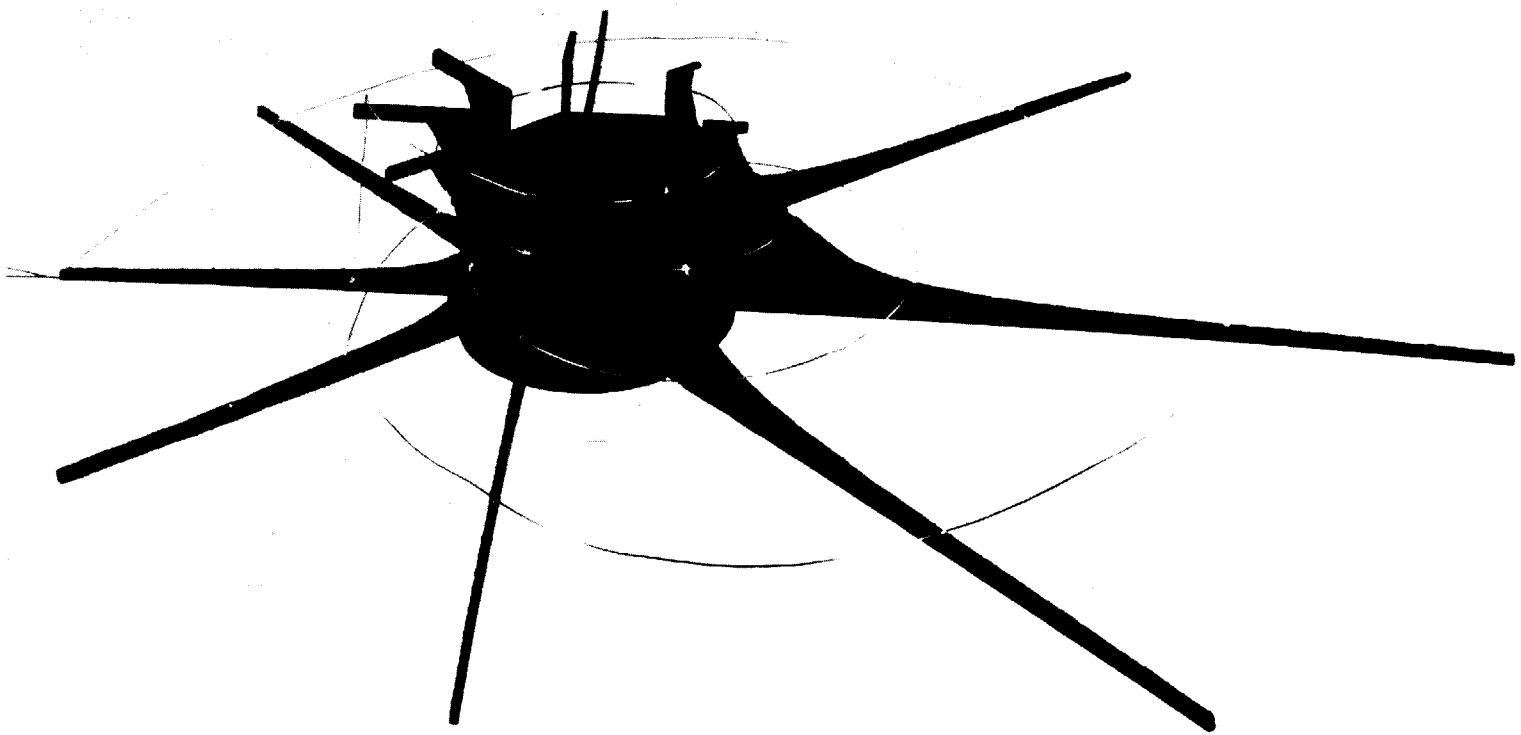

(c) $\mu = 0.030; \frac{V}{\Omega R\sqrt{\frac{1}{2} C_T}} \approx 0.65.$ L-60-292

Figure 4.- Concluded.

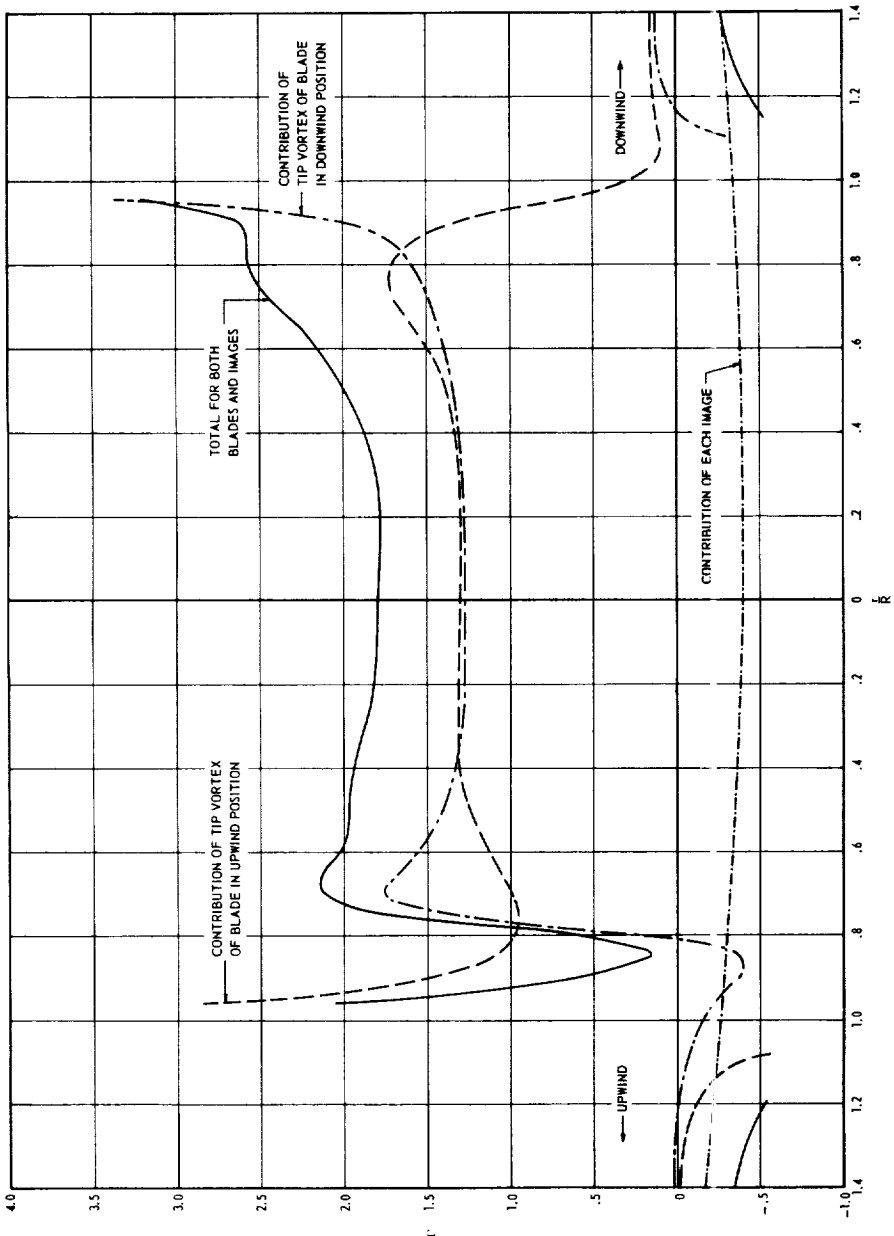

Figure 5.- Typical plot of electromagnetic-analog surveys in terms of nondimensional normal component of induced velocity associated with tip vortices for longitudinal diameter of tip path plane and for $\mu = 0.022$ or $\frac{V}{\Omega R\sqrt{\frac{1}{2}C_T}} \approx 0.48$.

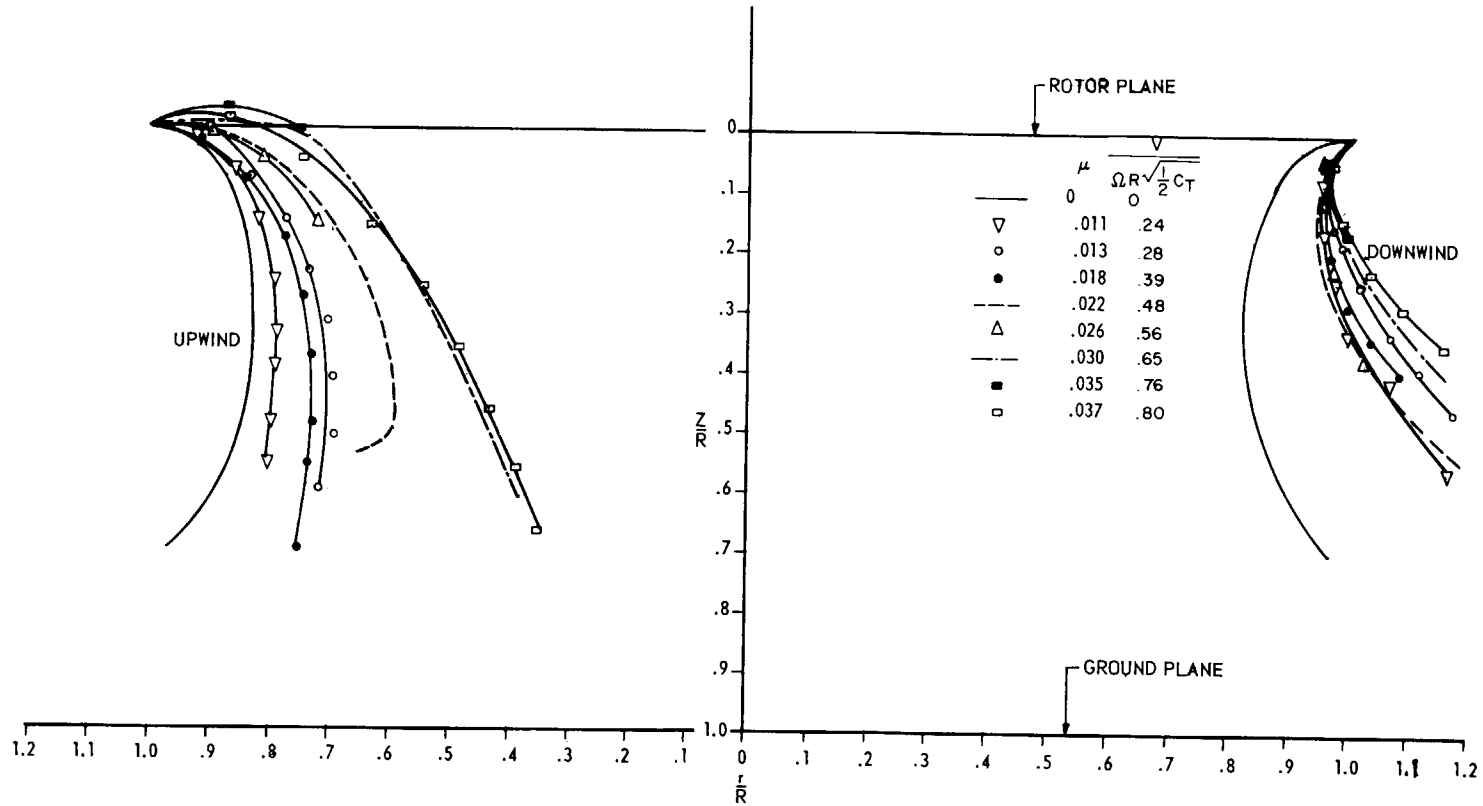

Figure 6.- Variation with advance ratio and ratio of forward velocity to calculated hovering induced velocity of nondimensional path of tip vortex in longitudinal plane of two-blade rotor operating in ground effect. Distance between each symbol represents 90° of blade rotation.

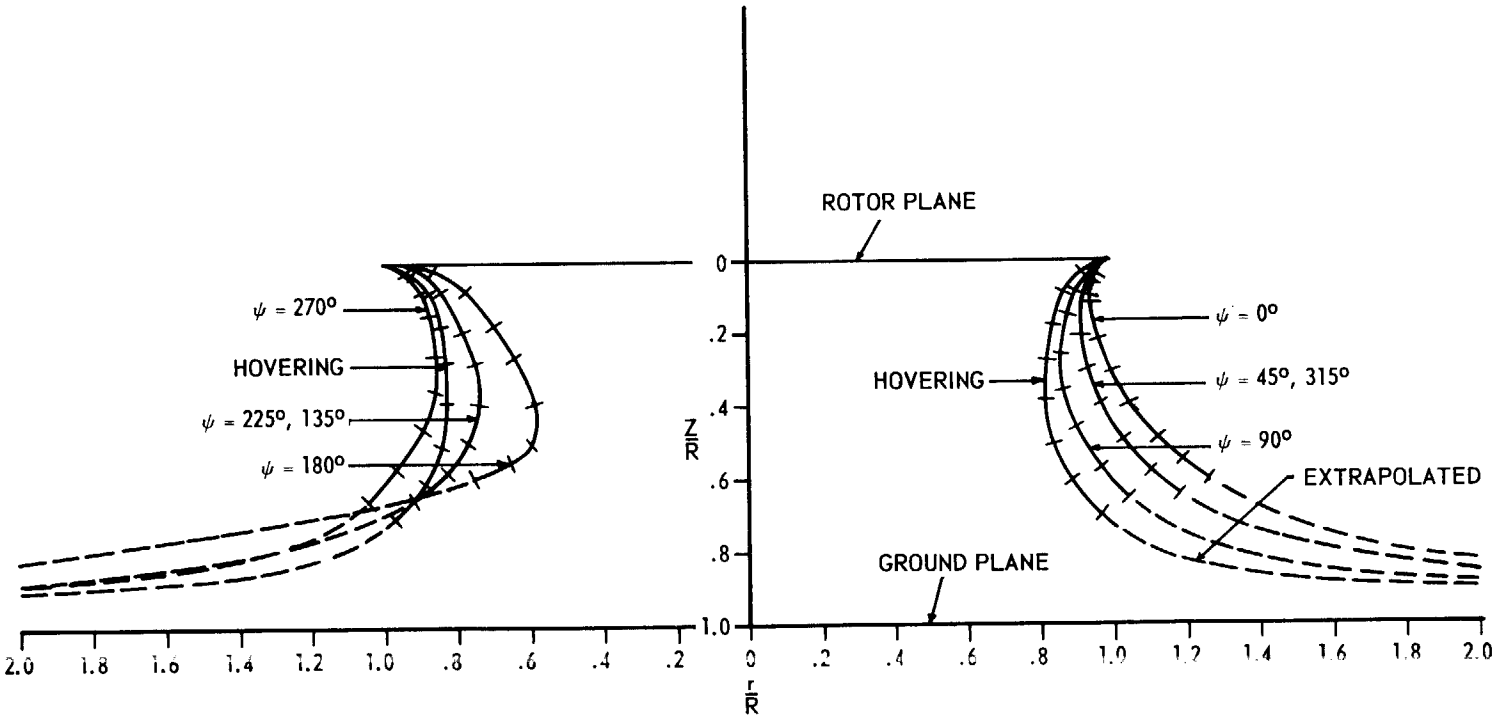

(a) Advance ratio $\mu = 0.022$ or $\frac{V}{\Omega R\sqrt{\frac{1}{2} C_T}} \approx 0.48$. Distance between each symbol represents 90° of blade rotation.

Figure 7.- Nondimensional paths of tip vortex in 45° interval planes and comparison with hovering flight. Cutting planes intersect at wake axis.

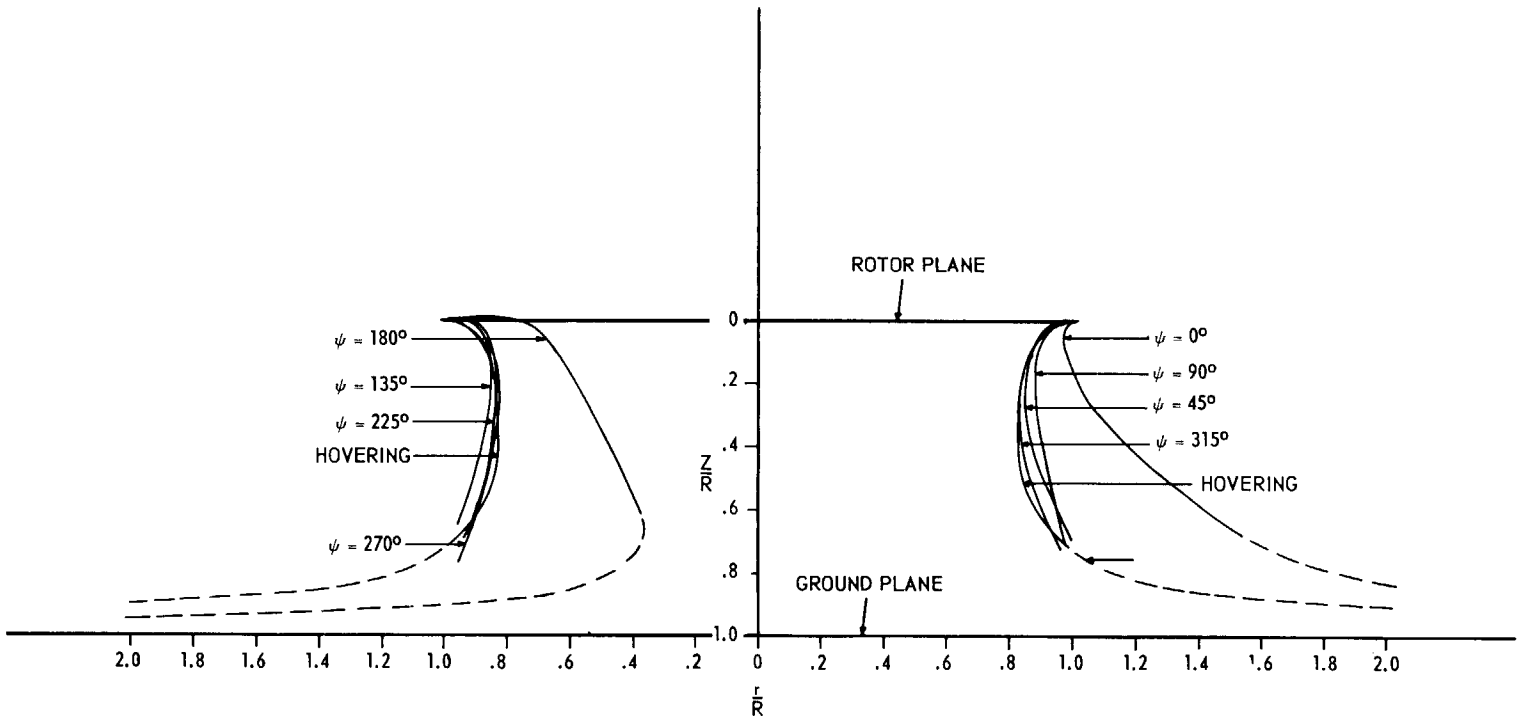

(b) Advance ratio $\mu = 0.030$ or $\dfrac{V}{\Omega R\sqrt{\frac{1}{2} C_T}} \approx 0.65$.

Figure 7.- Concluded.

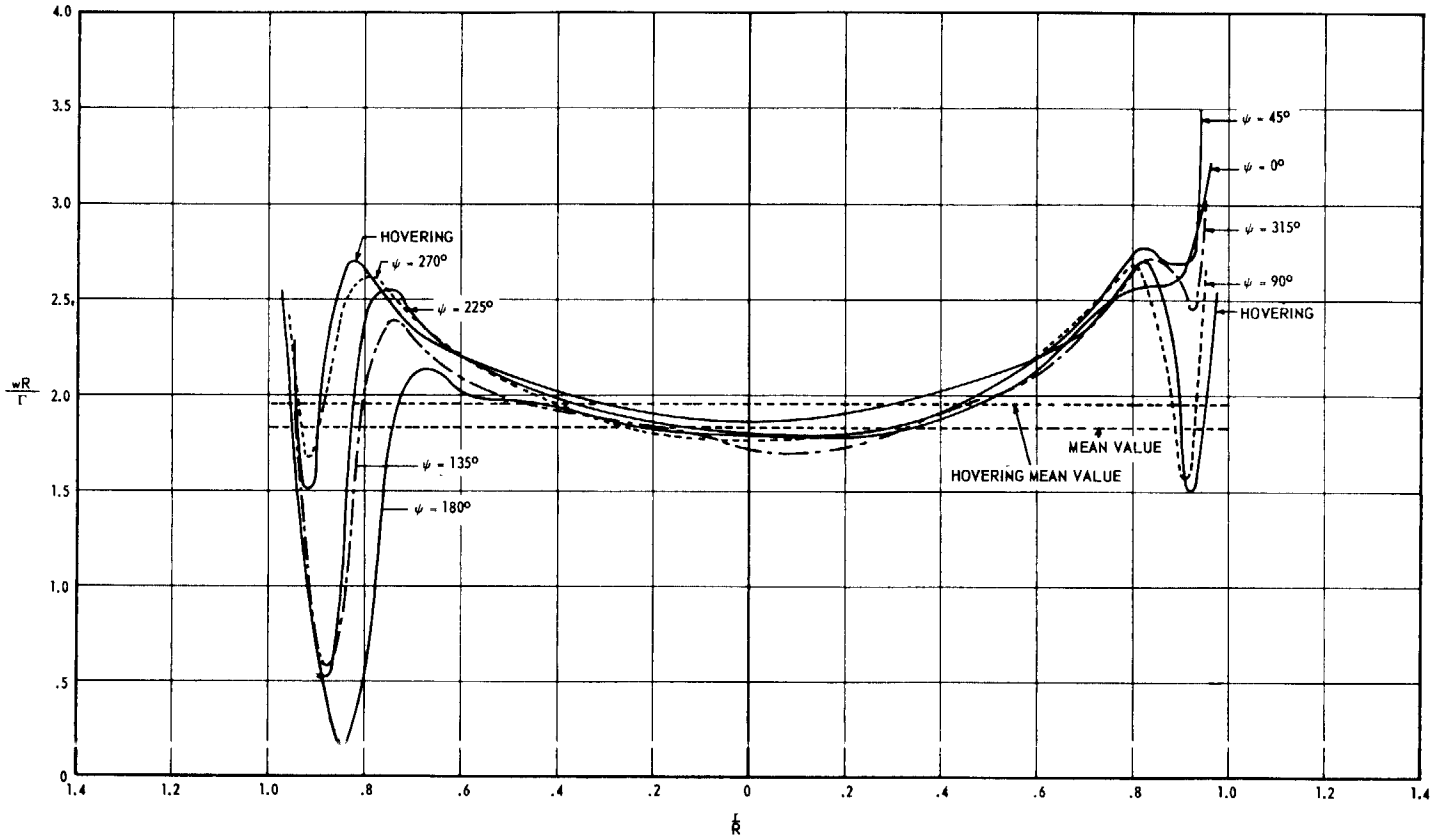

(a) $\mu = 0.022$; $\dfrac{V}{\Omega R\sqrt{\frac{1}{2}\,C_T}} \approx 0.48$; $\dfrac{Z}{R} = 1.00$; $\Gamma \approx \dfrac{3\pi\Omega R^2 C_T}{b}$ from reference 5.

Figure 8.- Nondimensional normal component of induced velocity associated with tip vortices along blade feathering axis of two-blade rotor in steady forward flight in ground effect and comparison with hovering.

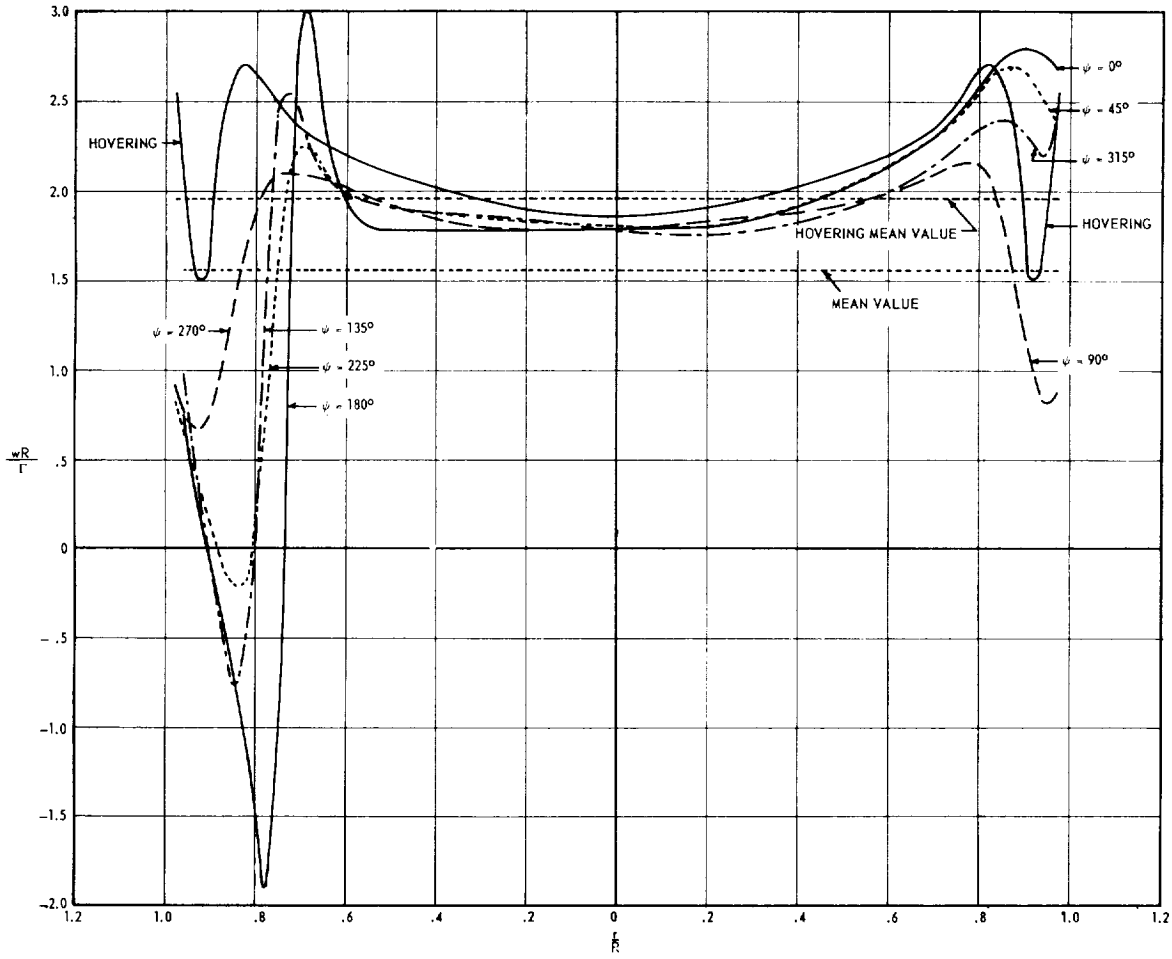

(b) $\mu = 0.030$; $\dfrac{V}{\Omega R\sqrt{\frac{1}{2}\,C_T}} \approx 0.65$; $\dfrac{Z}{R} = 1.00$; $\Gamma \approx \dfrac{3\pi\Omega R^2 C_T}{b}$ from reference 5.

Figure 8.- Concluded.

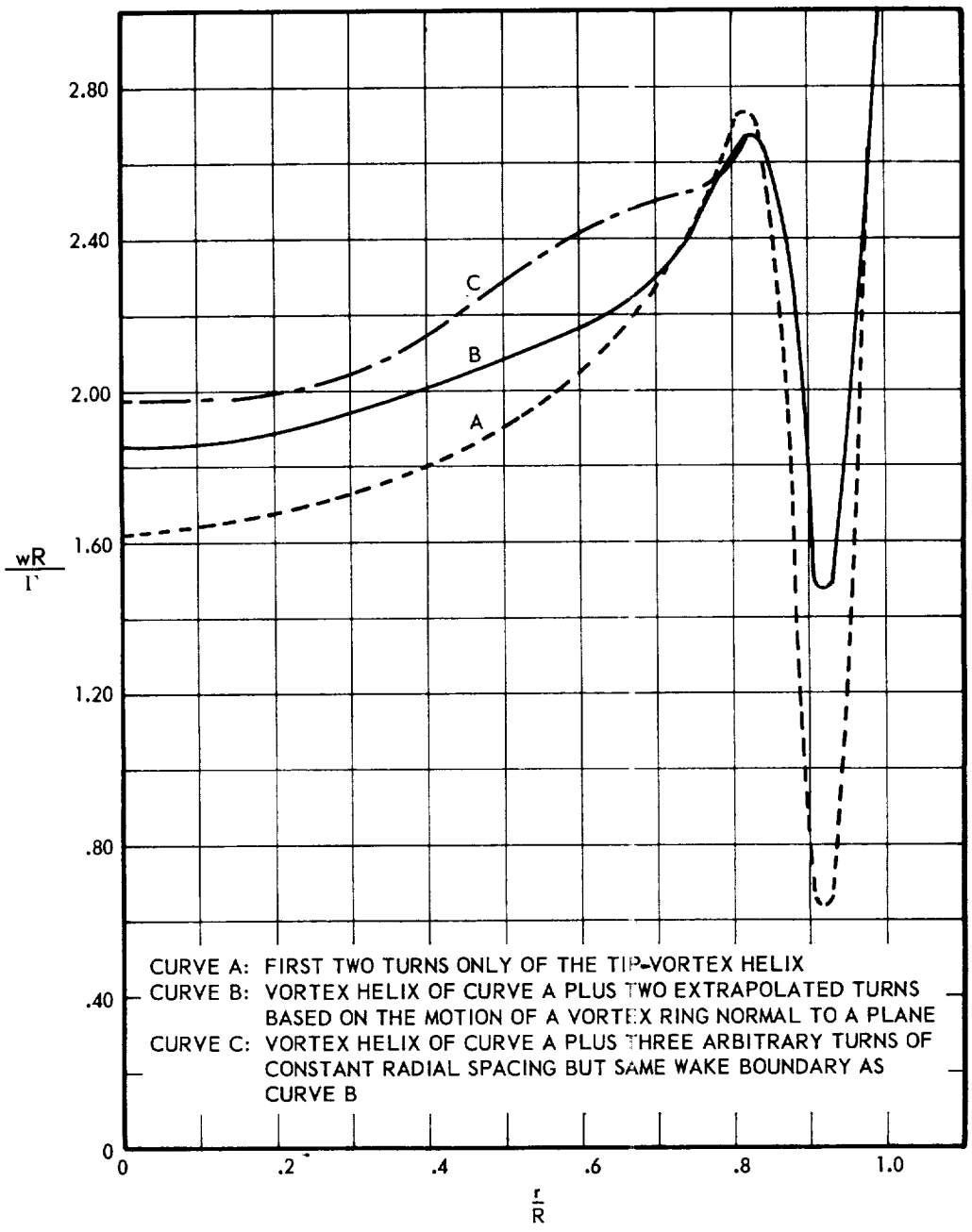

Figure 9.- Effect of extrapolated vortex coils on nondimensional axial induced velocity at blade pitch axis of a two-blade teetering rotor in hovering flight at a ground height of 1 rotor radius as measured on a magnetic model of wake tip vortex as determined from smoke studies of a model rotor wake. $\Gamma \approx \frac{3\pi\Omega R^2 C_T}{b}$ from reference 5.

W-143